

TOPOLOGY OPTIMIZATION OF 2D BUILDING FRAMES UNDER ARTIFICIAL EARTHQUAKE GROUND MOTIONS USING POLYGONAL FINITE ELEMENT METHOD

P. Zakian*,†

Department of Civil Engineering, Faculty of Engineering, Arak University, Arak, Iran

ABSTRACT

In this article, topology optimization of two-dimensional (2D) building frames subjected to seismic loading is performed using the polygonal finite element method. Artificial ground motion accelerograms compatible with the design response spectrum of ASCE 7-16 are generated for the response history dynamic analysis needed in the optimization. The mean compliance of structure is minimized as a typical objective function under the material volume fraction constraint. Also, the adjoint method is employed for the sensitivity analysis evaluated in terms of spatial and time discretization. The ground structures are 2D continua taking the main structural components (columns and beams) as passive regions (solid) to render planar frames with additional components. Hence, building frames with different aspect ratios are considered to assess the usefulness of the additional structural components when applying the earthquake ground motions. Furthermore, final results are obtained for different ground motions to investigate the effects of ground motion variability on the optimized topologies.

Keywords: Topology optimization; Dynamic loading; Response history analysis; Polygonal finite element method; Minimum compliance; Artificial earthquake accelerogram.

Received: 20 February 2023; Accepted: 30 March 2023

1. INTRODUCTION

Optimal design of structures under earthquake loads is an important and challenging issue in civil engineering, because providing an effective seismic performance considering the dynamic properties involved is not an easy problem. Also, this research area is relatively

^{*}Corresponding author: Department of Civil Engineering, Faculty of Engineering, Arak University, Arak, Iran

[†]E-mail address: p-zakian@araku.ac.ir (P. Zakian)

young, and is in a progressive state of development for more than two decades [1]. Current design methods are based on the traditional trial-and-error process guaranteeing structural safety, but these methods may not necessarily result in optimal designs. Therefore, numerous investigations on structural optimization have been carried out [1-7]. Topology optimization aims to optimize material distribution in a computational domain considering some objective function(s) and constraint(s) [8, 9]. The results of topology optimization can help engineers to design a lightweight, cheap, and high-performance structure. As deduced from modern building constructions, there are many inspirations initiated from topology optimization to find the most effective structural form against various loads in addition to new architectural forms [10-12]. In this regard, there are some applications of topology optimization providing conceptual designs for modern structures, such as Voronoi diagrams [10].

Many studies have been conducted in the field of topology optimization to develop effective formulations resolving the inherent numerical issues such as the checkerboard pattern, mesh dependency, local minima, etc. [9, 13-17]. Apart from numerous studies on static problems [18, 19], topology optimization has been applied to various dynamic problems including free and forced vibrations of solids and structures [20-23]. However, only a few studies on topology optimization directly considered earthquake loading which is one of the extreme loads sustained by structures [20, 24-26]. Although the structures subjected to strong ground motions are expected to undergo inelastic behavior, in most cases, the design procedure assumes linearly elastic behavior of the structure and indirectly implements the effects of nonlinearity. Therefore, many researchers have used linear analysis in the topology optimization of structures under seismic excitation [1, 24].

Here, the previous studies on topology optimization of structures considering earthquake loads are briefly discussed. Hajirasouliha et al. [27] optimized the topology of truss-like structures for seismic excitation to minimize the structural weight and to meet a state of uniform deformation. Zakian and Kaveh [26] proposed a topology optimization problem to identify the important structural parts of shear walls as well as shear wall-frame structures under both gravity and seismic loads using the equivalent static analysis. They also investigated the effects of structural tallness, shear wall-frame interaction, and opening. The Isotropic Material with Penalization (SIMP) approach was used to optimize compliance, and a penalty function was defined to impose a constraint on the top displacement. Allahdadian and Boroomand [24] performed topology optimization of a three-story planar frame subjected to seismic loads to minimize the norm of structural displacements. They employed the response history analysis using the finite element method with the SIMP approach. Gomez et al. [28] modeled the stochastic ground excitation as a zero-mean filtered white noise, and obtained the structural response covariances of 2D building models by solving the resulting Lyapunov equation. The optimization problem was introduced to minimize the maximum structural response covariances, and the sensitivities were calculated with a gradient-based solver. Martina and Deierlein [20] used a frequency-domain approach to propose a dynamic topology optimization formulation based on modal decompositions, by which the structural vibration was minimized for a seismic excitation defined as a response spectrum. Their results indicated that the optimized topology is affected by the earthquake frequency content.

The three-node and four-node elements are often used in two-dimensional finite element

models. Nevertheless, a generalized element like the polygonal element with more than four vertices leads to further developments in mesh generation and the finite element method [29]. Indeed, polygonal finite elements can provide higher flexibility for the meshing of complicated geometries (see Figure 1). In this article, topology optimization of building frames under earthquake ground motion is considered using the polygonal finite element method. Artificial ground motion accelerograms are generated using the design spectrum of ASCE 7-16 [30] for the dynamic analysis needed in optimal seismic design. Topology optimization is carried out to minimize the mean compliance of structure considering the constraint of material volume fraction. Also, the adjoint method is employed for the sensitivity analysis. Two building frames with different aspect ratios are selected as the ground structures to evaluate the effectiveness of various structural parts under earthquake excitations. Different designs of structural topology corresponding to the generated accelerograms are obtained to include the effects of ground motion variability.

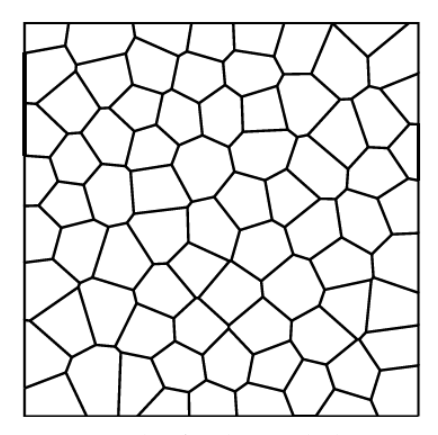


Figure 1. A mesh of polygonal elements [29].

The remaining part of this article is organized as follows: Section 2 describes the topology optimization problem, and contains an overview of the applied solution method for topology optimization of the structure under seismic loading. Section 3 describes the artificially generated earthquake accelerograms. In Section 4, the results of two examples are provided. Finally, Section 5 summarizes the concluding remarks.

2. TOPOLOGY OPTIMIZATION FORMULATION

In this section, theoretical aspects of topology optimization in linear elasticity incorporating the dynamic loading are presented. Also, the design domain and density field utilized in the formulations of the optimization problem are briefly discussed, as implemented in PolyDyna [31]. In this study, the PolyDyna with slight modifications is used.

2.1 Problem description

The governing equation of a linearly elastic dynamic problem can be stated as:

$$\mathbf{div}\boldsymbol{\sigma} + \mathbf{b} = \bar{\rho}\,\ddot{\mathbf{u}} + \bar{c}\,\dot{\mathbf{u}}, \quad \text{in } \Omega$$

$$\mathbf{u} = \overline{\mathbf{u}}, \quad \text{on } \Gamma_{\mathrm{D}}$$

$$\boldsymbol{\sigma}.\mathbf{n} = \mathbf{t}, \quad \text{on } \Gamma_{\mathrm{N}}$$
(1)

where σ , t, b, \ddot{u} , \dot{u} and u show the stress tensor, prescribed boundary tractions, body force field, acceleration field, velocity field, and displacement field, respectively; \bar{c} is a damping factor leading to energy dissipation. Also, \mathbf{n} indicates the unit outward normal vector. The stress tensor is calculated using the linear isotropic elasticity tensor and the infinitesimal strain tensor, as given by

$$\sigma = \mathbf{C} : \varepsilon,$$

$$\varepsilon = \frac{1}{2} (\nabla \mathbf{u} + \nabla \mathbf{u}^{\mathrm{T}})$$
(2)

In the topology optimization, the elasticity tensor depends on a density field which can be introduced using either the SIMP or Rational Approximation of Material Properties (RAMP). Furthermore, $\bar{\rho}$ denotes the physical density at point $\mathbf{x} \in \Omega$, which is usually expressed in terms of the density field, that is

$$\bar{\rho} = m_{V}(\rho)\rho_{0} \tag{3}$$

in which ρ_0 and $m_V(\rho)$ denote the mass density of solid material and volume interpolation function corresponding to the volume fraction at point \mathbf{x} . The statement in Eq. (1) is valid for topology optimization of continua with arbitrary objective and constraint functions. However, in this paper, the objective function is the mean compliance of structure, as given by

$$f(\rho, \mathbf{u}) = \frac{1}{t_f} \int_0^{t_f} \int_{\Gamma_N} \mathbf{t} \cdot \mathbf{u} \, d\mathbf{x} dt$$
 (4)

In addition, in order to impose a limitation on the amount of material, the following constraint is defined:

$$g(\rho) = \frac{1}{|\Omega|} \int_{\Omega} m_V(\rho) d\mathbf{x} - \overline{V} \le 0$$
 (5)

where \bar{v} denotes the prescribed total material volume fraction.

2.2 Discretization

Let \mathbf{z} be the vector of design variables, such that $\mathbf{z} \in [0, 1]^N$ where N shows the total number of design variables which is also equal to the total number of polygonal elements used in the mesh. Hence, the vector of filtered densities is expressed as

$$\mathbf{y} = \mathbf{P}\mathbf{z} \tag{6}$$

in which **P** is the filter matrix computed by

$$P_{lk} = \frac{w_{lk} A_{k}}{\sum_{j=1}^{N} w_{lj} A_{j}}$$
 (7)

with A_k being the element area; and w_{lk} is a weighting coefficient based on the selected filter kernel.

Furthermore, the time discretization of the governing equation using N_t time steps leads to

$$\mathbf{M}\ddot{\mathbf{u}}_{i} + \mathbf{C}\dot{\mathbf{u}}_{i} + \mathbf{K}\mathbf{u}_{i} = \mathbf{f}_{i}, \quad i = 0, 1, ..., N_{t}$$
(8)

where **M**, **C**, and **K** are mass, damping, and stiffness matrices, respectively. Also, \mathbf{f}_i , $\ddot{\mathbf{u}}_i$, and \mathbf{u}_i are force, acceleration, velocity, and displacement vectors at the *i*th time step, respectively. When considering an earthquake excitation, $\mathbf{f}_i = -\mathbf{Mr}\ddot{u}_i^g$ where **r** is the influence coefficient vector, and \ddot{u}_i^g is the ground acceleration at the *i*th time step. For a horizontal earthquake excitation, $\mathbf{r} = [1, 0, 1, 0, ..., 1, 0]^T$ is considered when using two-dimensional polygonal elements. Mass and stiffness matrices are evaluated as

$$\mathbf{M} = \sum_{l=1}^{N} \tilde{m}_{V}(y_{l})\mathbf{m}_{l}$$

$$\tag{9}$$

and

$$\mathbf{K} = \sum_{l=1}^{N} \tilde{m}_{E}(\mathbf{y}_{l}) \mathbf{k}_{l} \tag{10}$$

where the summation refers to the assembly operator. Also, the mass matrix and stiffness matrix of an element are calculated by

$$\mathbf{m}_{l} = \int_{\Omega_{l}} \rho_{0} \mathbf{H}_{l}^{\mathrm{T}} \mathbf{H}_{l} d\mathbf{x}$$
 (11)

and

$$\mathbf{k}_{l} = \int_{\Omega_{l}} \mathbf{B}_{l}^{\mathrm{T}} \mathbf{C}_{0} \mathbf{B}_{l} d\mathbf{x}$$
 (12)

in which \mathbf{H}_i and \mathbf{B}_i indicate the interpolation functions matrix and the strain-displacement matrix, respectively. Also, \mathbf{C}_0 is the moduli matrix for a linearly elastic material.

The volume and material interpolation functions are obtained as

$$\tilde{m}_{V}(y_{I}) = \varepsilon + (1 - \varepsilon)m_{V}(y_{I}) \tag{13}$$

and

$$\tilde{m}_{E}(y_{1}) = \varepsilon + (1 - \varepsilon)m_{E}(y_{1}) \tag{14}$$

in which $\varepsilon \ll 1$ to avoid instability when y_t approaches zero in the limit. Here, the threshold interpolation function and the RAMP function are used as the volume and material interpolation functions, respectively [32, 33]. Moreover, the damping matrix is computed using the Rayleigh approach, as follows:

$$\mathbf{C} = a_M \mathbf{M} + a_K \mathbf{K} \tag{15}$$

in which $a_{\scriptscriptstyle M}$ and $a_{\scriptscriptstyle K}$ are two parameters depending on the damping ratios and the natural frequencies of effective modes.

According to the discretization of both density and displacement fields, the discretized elastodynamic topology optimization problem is obtained as follows:

Minimize
$$f(\mathbf{z}, \mathbf{u}_0, ..., \mathbf{u}_{N_t})$$

such that $g_j(\mathbf{z}) = \frac{\sum_{l \in \ell_j} A_l \tilde{m}_V(y_l)}{\sum_{l \in \ell_j} A_l} - \bar{v}_j \le 0,$ $j = 1, ..., N_c$ (16)

 $\mathbf{M}\ddot{\mathbf{u}}_i + \mathbf{C}\dot{\mathbf{u}}_i + \mathbf{K}\mathbf{u}_i = \mathbf{f}_i, \quad i = 0, 1, ..., N_t$

in which A_l is the area of the *l*th element, N_c is the number of volume constraints, and ℓ_j denotes a set of elements constrained by g_j . Also, the discrete form of mean dynamic compliance is stated as

$$f\left(\mathbf{z},\mathbf{u}_{0},...,\mathbf{u}_{N_{t}}\right) = \frac{1}{N_{t}} \sum_{i=0}^{N_{t}} \mathbf{f}_{i}^{\mathsf{T}} \mathbf{u}_{i}$$

$$(17)$$

It should be noted that the Hilber, Hughes, and Taylor (HHT- α) scheme [34] is used for the time integration here.

2.3 Sensitivity analysis

In this study, the adjoint method is utilized for sensitivity analysis to prevent the calculation of expensive derivatives of the state variables. Accordingly, the *discretize-then-differentiate* approach is used [31, 35].

The sensitivity of an objective function is expressed as

$$\frac{\mathrm{d}f}{\mathrm{d}z_{e}} = \frac{\partial f}{\partial z_{e}} + \sum_{i=0}^{N_{t}} \frac{\partial f}{\partial \mathbf{u}_{i}} \cdot \frac{\partial \mathbf{u}_{i}}{\partial z_{e}}$$
(18)

Indeed, in order to prevent the computational efforts needed for calculating the last term in Eq. (18), the adjoint method is used. Using the HHT- α method for the time discretization, and after some algebraic operations, the following relation is obtained [31]:

$$\frac{\mathrm{d}f}{\mathrm{d}z_{e}} = \sum_{l=1}^{N} \left(\frac{\partial E_{l}}{\partial z_{e}} \cdot \frac{\mathrm{d}f}{\mathrm{d}E_{l}} + \frac{\partial V_{l}}{\partial z_{e}} \cdot \frac{\mathrm{d}f}{\mathrm{d}V_{l}} \right)$$
(19)

with

$$\frac{\mathrm{d}f}{\mathrm{d}E_{I}} = \frac{\partial f}{\partial E_{I}} + \sum_{i=0}^{N_{I}} \xi_{i}^{\mathrm{T}} \frac{\partial \mathbf{R}_{i}}{\partial E_{I}}$$
(20)

and

$$\frac{\mathrm{d}f}{\mathrm{d}V_{l}} = \frac{\partial f}{\partial V_{l}} + \sum_{i=0}^{N_{i}} \xi_{i}^{\mathrm{T}} \frac{\partial \mathbf{R}_{i}}{\partial V_{l}}$$
(21)

in which ξ_i^T and \mathbf{R}_i are the adjoint vector and residual vector at the *i*th time step, such that

$$\frac{\partial \mathbf{R}_{i}}{\partial E_{l}} = \begin{cases} \mathbf{k}_{l} \left(\mathbf{u}_{l0} + a_{K} \dot{\mathbf{u}}_{l0} \right) & for \ i = 0 \\ \mathbf{k}_{l} \left[(1 - \alpha) \left(\mathbf{u}_{li} + a_{K} \dot{\mathbf{u}}_{li} \right) + \alpha \left(\mathbf{u}_{l(i-1)} + a_{K} \dot{\mathbf{u}}_{l(i-1)} \right) \right] & for \ i = 1, ..., N_{t} \end{cases}$$
(22)

[DOI: 10.22068/ijoce.2023.13.3.554]

P. Zakian

and

$$\frac{\partial \mathbf{R}_{i}}{\partial V_{l}} = \begin{cases} \mathbf{m}_{l} (\ddot{\mathbf{u}}_{l0} + a_{M} \dot{\mathbf{u}}_{l0}) & for \ i = 0 \\ \mathbf{m}_{l} \left[\ddot{\mathbf{u}}_{li} + a_{M} \left((1 - \alpha) \dot{\mathbf{u}}_{li} + \alpha \dot{\mathbf{u}}_{l(i-1)} \right) \right] & for \ i = 1, ..., N_{t} \end{cases}$$
(23)

where α is a parameter in the HHT- α scheme. For the mean dynamic compliance as the objective function when considering the earthquake excitation, one can write

$$\frac{\partial f}{\partial E_l} = 0, \qquad \frac{\partial f}{\partial V_l} = -\sum_{l=1}^{N} \sum_{i=0}^{N_t} (\mathbf{m}_l \mathbf{r}_l \ddot{u}_i^g)^T \mathbf{u}_{li}, \qquad \frac{\partial f}{\partial \mathbf{u}_i} = \frac{-1}{N_t} \mathbf{M} \mathbf{r} \ddot{u}_i^g$$
(24)

where \mathbf{u}_{ii} denotes the displacement vector corresponding to element l at the ith time step.

3. ARTIFICIAL EARTHQUAKE ACCELEROGRAMS

In this section, the employed earthquake accelerograms are discussed. The use of artificial ground motions can reduce the computational cost because the total number of time steps for an artificial ground motion can usually be less than that of a real ground motion. However, when the ground motion is compatible with a design spectrum, as an alternative to the real ground motion, the artificial ground motion can also give desirable results due to its reasonable frequency content and peak ground acceleration (PGA). In order to consider the effects of ground motion variability and the effects of using almost the same intensity for ground motions in the topology optimization problem, three artificial ground motions compatible with the design spectrum of ASCE 7-16 [30] are generated. The method given in Ref. [36] is used for synthesized accelerogram generation, and also the quadratic baseline correction is employed for the accelerograms. In the definition of the design spectrum illustrated in Figure 2, the site class D and spectral response acceleration parameters S_s =0.60g and S_I =0.32g are assumed.

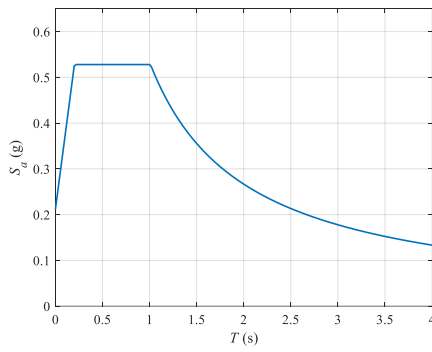


Figure 2. The design response spectrum used for synthesized accelerogram generation.

Also, the long-period transition period and the moment magnitude are taken as T_L =8 s and M_w =6.5. The generated accelerograms are shown in Figure 3 where the PGA of the first,

second, and third accelerograms are equal to 0.246g, 0.241g, and 0.288g, respectively.

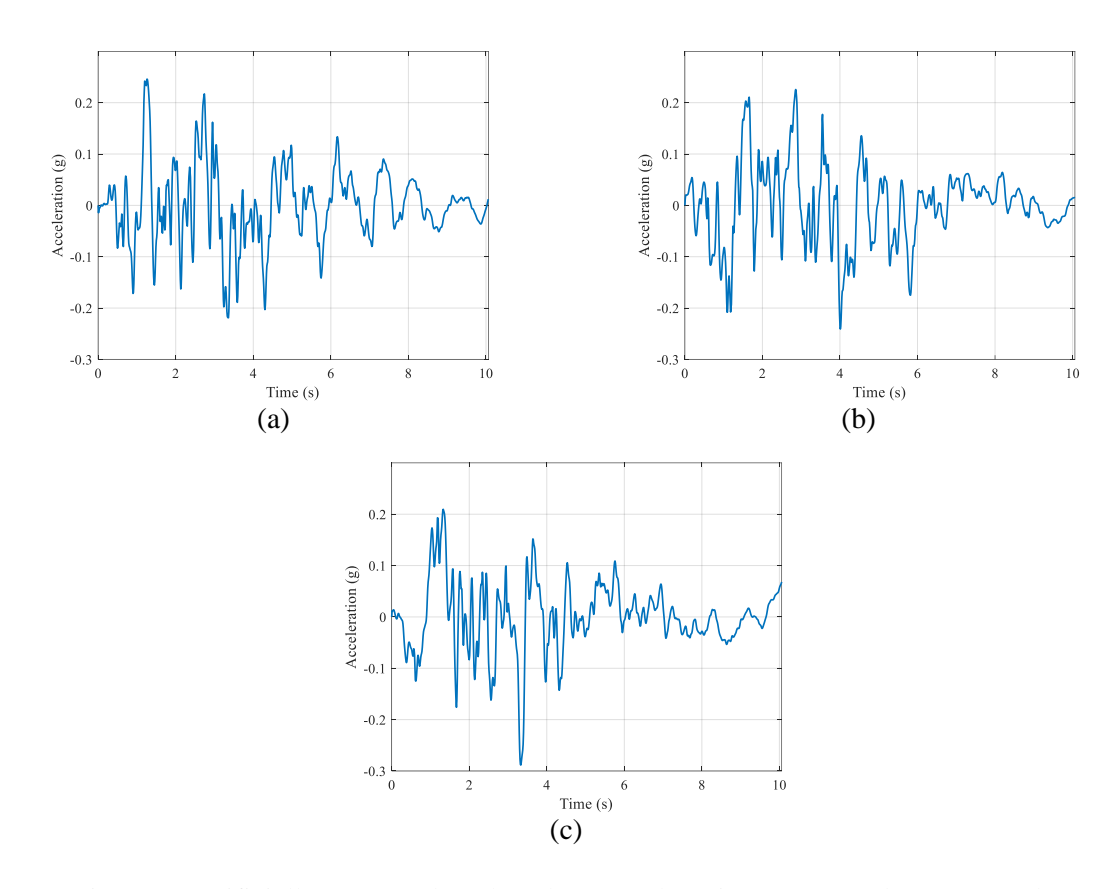


Figure 3. Artificially generated earthquake ground motions: (a) Accelerogram 1, (b) Accelerogram 2, and (c) Accelerogram 3.

4. DESIGN EXAMPLES

This section presents two examples of topology optimization for two-dimensional building frames under artificial ground motions using the response history analysis. The ground structures are two-dimensional continua (see Figure 4) containing passive regions to render building frames having additional structural components. These passive regions include the columns and beams as the main structural components which are not removed from the domain (passive solid region) during the optimization.

In-plane dimensions of columns and beams are selected as 0.4~m. For all the examples, the damping ratio is chosen as 0.05, and the volume fraction limit is taken as 0.35. Elasticity modulus, mass density, and Poisson ratio are assumed to be 35 GPa, $2400~\text{kg/m}^3$, and 0.2, respectively. In addition, a lumped mass of 5000~kg is assigned to both end nodes of every beam in the structure. Each generated accelerogram has a duration of 10.06~s, which is applied to the structure in the horizontal direction, as shown in Figure 4. The time step size of dynamic analysis is equal to that of the accelerograms, which is 0.01~s.

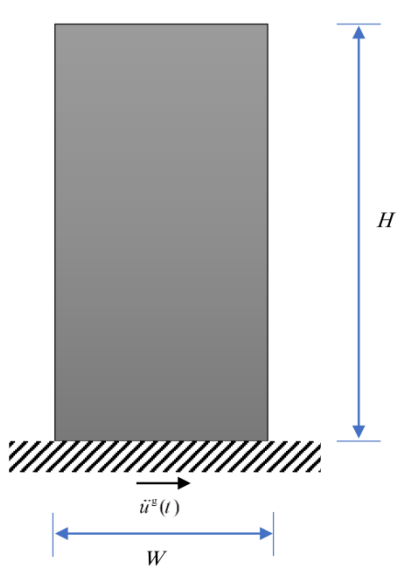


Figure 4. The ground structure used in topology optimization under a horizontal earthquake excitation.

4.1 Low-rise case

The first example is a low-rise building frame. The width and height of the structure are selected as 4.8 m and 6.6 m, respectively. Damping coefficients are $a_M = 2.0904$ and $a_K = 3.9535 \times 10^{-4}$, and a mesh of 12,672 elements with unit thickness is used. Also, the filter radius is assumed as 0.1 m. Results of the topology optimization are illustrated in Figure 5, demonstrating that using the employed ground motions leads to almost the same designs. This phenomenon can be due to using the same design spectrum for generating those three ground motions. Furthermore, the configuration of the required bracings for the first story is different from that of the second story.

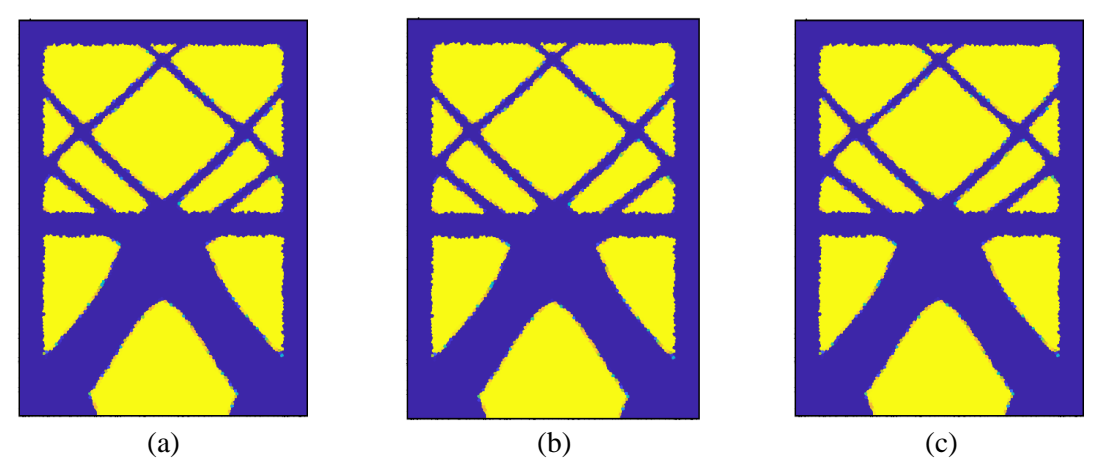


Figure 5. Optimized topologies obtained for the low-rise case using different earthquake ground motions: (a) Accelerogram 1, (b) Accelerogram 2, and (c) Accelerogram 3.

4.2 Mid-rise case

Here, a four-story frame with a width of 4.8 m and a height of 13 m is considered. Damping coefficients are a_M =1.1357 and a_K =7.2769×10⁻⁴, and a mesh of 24,960 elements with unit thickness is used. The filter radius is equal to 0.2 m. The optimized topologies for three ground motions are illustrated in Figure 6. The optimized designs obtained using accelerograms 1 and 2 are almost the same, but the design optimized using accelerogram 3 is slightly different from them in the higher stories because the bracings in higher stories have larger lengths (located in higher elevations) when using accelerogram 3. Furthermore, size of the bracing connections formed in the third story in Figure 6(c) is not very similar to the corresponding sizes in Figures 6(a) and 6(b). Similar to the previous example, the lower stories require significantly stronger bracings than the higher stories.

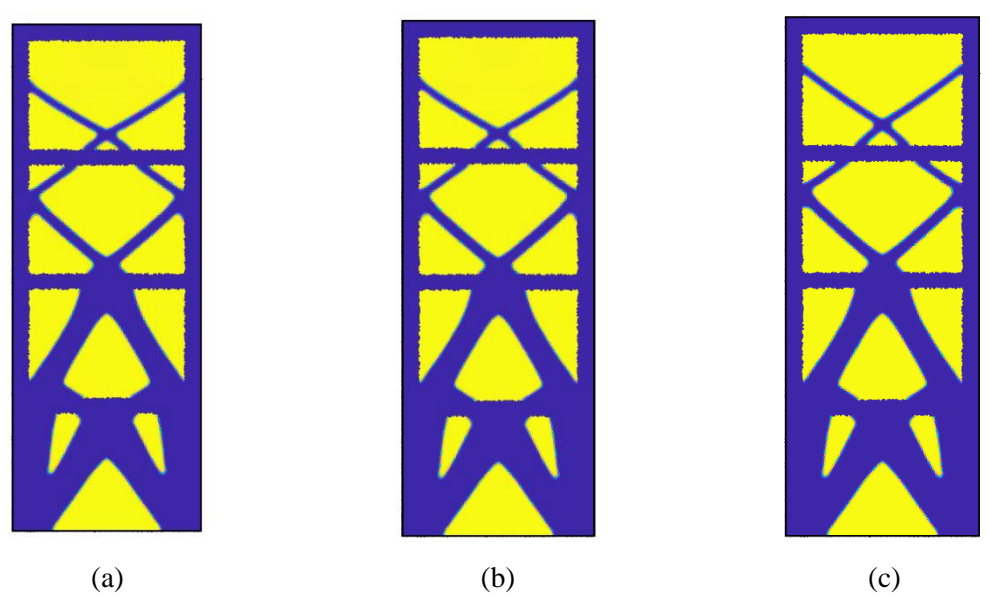


Figure 6. Optimized topologies obtained for the mid-rise case using different earthquake ground motions: (a) Accelerogram 1, (b) Accelerogram 2, and (c) Accelerogram 3.

5. CONCLUSOINS

In this paper, topology optimization of planar continua under seismic excitation was performed using the linear response history analysis. In order to improve the applicability of optimized solutions, building frames corresponding to the planar continua were generated by defining the passive solid regions. The polygonal finite element method was utilized for spatial discretization, due to its suitable performance in modeling complex geometries. Also, the HHT- α scheme was used as the time integration, and artificial ground motion accelerograms were generated according to the ASCE 7-16 design spectrum for the dynamic analysis.

Three ground motions were employed in order to evaluate the effects of ground motion variability on the optimized topologies obtained by minimizing the mean dynamic compliance under a constraint on the material volume fraction. The final results provide

desirable insight into the topological properties of the structure in both architectural and structural aspects. Also, the optimized topologies illustrate that the differences between the results obtained using the employed accelerograms are not significant when considering the ground motions compatible with the design spectrum. Of course, the differences are greater for the mid-rise structure. Since the dynamic properties of low-rise and mid-rise structures are not identical, one can obviously expect different optimized topologies as demonstrated by the examples. However, the obtained results similarly show that low elevations of the structure need remarkably stronger bracings than its high elevations.

REFERENCES

- 1. Zakian P, Kaveh A. Seismic design optimization of engineering structures: a comprehensive review. *Acta Mech.* 2023; **234**: 1305-30.
- 2. Rahami H, Kaveh A, Gholipour Y. Sizing, geometry and topology optimization of trusses via force method and genetic algorithm. *Eng Struct*. 2008; **30**: 2360-9.
- 3. Zakian P. Meta-heuristic design optimization of steel moment resisting frames subjected to natural frequency constraints. *Adv Eng Softw.* 2019; **135**: 102686.
- 4. Zakian P. Design optimization of moment frame structures based on natural frequency constraints using the adaptive charged system search algorithm. *Int J Optim Civil Eng.* 2021; **11**: 581-97.
- 5. Kaveh A. Advances in Metaheuristic Algorithms for Optimal Design of Structures: Springer; 2021.
- 6. Kaveh A. Applications of Metaheuristic Optimization Algorithms in Civil Engineering: Springer; 2016.
- 7. Kaveh A, Zakian P. Enhanced bat algorithm for optimal design of skeletal structures. *Asian J Civil Eng.* 2014; **15**: 179-212.
- 8. Bendsøe MP, Kikuchi N. Generating optimal topologies in structural design using a homogenization method. *Comput Methods Appl Mech Eng.* 1988; **71**: 197-224.
- 9. Hassani B, Hinton E. A review of homogenization and topology optimization III—topology optimization using optimality criteria. *Comput Struct*. 1998; **69**: 739-56.
- 10. Beghini LL, Beghini A, Katz N, Baker WF, Paulino GH. Connecting architecture and engineering through structural topology optimization. *Eng Struct*. 2014; **59**: 716-26.
- 11. Stromberg LL, Beghini A, Baker WF, Paulino GH. Topology optimization for braced frames: Combining continuum and beam/column elements. *Eng Struct*. 2012; **37**: 106-24.
- 12. Zegard T, Paulino GH. Bridging topology optimization and additive manufacturing. *Struct Multidiscip Optim.* 2016; **53**: 175-92.
- 13. Bendsoe MP, Sigmund O. Topology Optimization: Theory, Methods, and Applications: Springer; 2004.
- 14. Sigmund O, Maute K. Topology optimization approaches. *Struct Multidiscip Optim*. 2013; **48**: 1031-55.
- 15. Huang X, Xie Y-M. A further review of ESO type methods for topology optimization. *Struct Multidiscip Optim.* 2010; **41**: 671-83.
- 16. Liu J, Ma Y. A survey of manufacturing oriented topology optimization methods. Adv

- Eng Softw. 2016; 100: 161-75.
- 17. Rozvany GIN. A critical review of established methods of structural topology optimization. *Struct Multidiscip Optim*. 2009; **37**: 217-37.
- 18. Kaveh A, Hassani B, Shojaee S, Tavakkoli SM. Structural topology optimization using ant colony methodology. *Eng Struct*. 2008; **30**: 2559-65.
- 19. Tavakkoli S, Hassani B. Isogeometric topology optimization by using optimality criteria and implicit function. *Int J Optim Civil Eng.* 2014;4:151-63.
- 20. Martin A, Deierlein GG. Structural topology optimization of tall buildings for dynamic seismic excitation using modal decomposition. *Eng Struct*. 2020; **216**: 110717.
- 21. Zargham S, Ward TA, Ramli R, Badruddin IA. Topology optimization: a review for structural designs under vibration problems. *Struct Multidiscip Optim*. 2016; 53: 1157-77.
- 22. Kang B-S, Park G-J, Arora JS. A review of optimization of structures subjected to transient loads. *Struct Multidiscip Optim*. 2006; **31**: 81-95.
- 23. Yaghoobi N, Hassani B. Topological optimization of vibrating continuum structures for optimal natural eigenfrequency. *Int J Optim Civil Eng.* 2017; **7**: 1-12.
- 24. Allahdadian S, Boroomand B. Topology optimization of planar frames under seismic loads induced by actual and artificial earthquake records. *Eng Struct*. 2016; **115**: 140-54.
- 25. Angelucci G, Quaranta G, Mollaioli F. Topology optimization of multi-story buildings under fully non-stationary stochastic seismic ground motion. *Struct Multidiscip Optim*. 2022; **65**: 217.
- 26. Zakian P, Kaveh A. Topology optimization of shear wall structures under seismic loading. *Earthq Eng Eng Vib.* 2020; **19**: 105-16.
- 27. Hajirasouliha I, Pilakoutas K, Moghaddam H. Topology optimization for the seismic design of truss-like structures. *Comput Struct*. 2011; **89**: 702-11.
- 28. Gomez F, Spencer BF, Carrion J. Topology optimization of buildings subjected to stochastic base excitation. *Eng Struct*. 2020; **223**: 111111.
- 29. Sukumar N, Malsch EA. Recent advances in the construction of polygonal finite element interpolants. *Arch Comput Methods Eng.* 2006; **13**: 129-63.
- 30. ASCE. Minimum Design Loads and Associated Criteria for Buildings and Other Structures: ASCE/SEI 7-16. 2016.
- 31. Giraldo-Londoño O, Paulino GH. PolyDyna: a Matlab implementation for topology optimization of structures subjected to dynamic loads. *Struct Multidiscip Optim*. 2021; **64**: 957-90.
- 32. Stolpe M, Svanberg K. An alternative interpolation scheme for minimum compliance topology optimization. S *Struct Multidiscip Optim*. 2001; **22**: 116-24.
- 33. Wang F, Lazarov BS, Sigmund O. On projection methods, convergence and robust formulations in topology optimization. *Struct Multidiscip Optim.* 2011; **43**: 767-84.
- 34. Hilber HM, Hughes TJR, Taylor RL. Improved numerical dissipation for time integration algorithms in structural dynamics. *Earthq Eng Struct Dyn.* 1977; **5**: 283-92.
- 35. Jensen JS, Nakshatrala PB, Tortorelli DA. On the consistency of adjoint sensitivity analysis for structural optimization of linear dynamic problems. *Struct Multidiscip Optim.* 2014; **49**: 831-7.
- 36. Halldorsson B, Papageorgiou AS. Calibration of the Specific Barrier Model to Earthquakes of Different Tectonic Regions. *Bull Seismol Soc Am.* 2005; **95**: 1276-300.